ISSN 1063-780X, Plasma Physics Reports, 2015, Vol. 41, No. 11, pp. 882–894. © Pleiades Publishing, Ltd., 2015.
Original Russian Text © S.A. Dan'ko, K.N. Mitrofanov, V.I. Krauz, V.V. Myalton, A.I. Zhuzhunashvili, V.P. Vinogradov, A.M. Kharrasov, S.S. Anan'ev, Yu.V. Vinogradova, Yu.G. Kalinin, 2015, published in Fizika Plazmy, 2015, Vol. 41, No. 11, pp. 955–968.

PLASMA DYNAMICS

Study of Soft X-Ray Emission during Wire Array Implosion under Plasma Focus Conditions at the PF-3 Facility

S. A. Dan'ko[a], K. N. Mitrofanov[b], V. I. Krauz[a], V. V. Myalton[a], A. I. Zhuzhunashvili[a], V. P. Vinogradov[a], A. M. Kharrasov[a], S. S. Anan'ev[a], Yu. V. Vinogradova[a], and Yu. G. Kalinin[a]

[a] *National Research Centre Kurchatov Institute, pl. Akademika Kurchatova 1, Moscow, 123182 Russia*
[b] *Troitsk Institute for Innovation and Fusion Research, Troitsk, Moscow, 142190 Russia*
e-mail: mitrofan@triniti.ru

Received May 13, 2015; in final form, June 10, 2015

Abstract—Results of measurements of soft X-ray emission with photon energies of <1 keV under conditions of a plasma focus (PF) experiment are presented. The experiments were carried out at the world's largest PF device—the PF-3 Filippov-type facility ($I \leqslant 3$ MA, $T/4 \approx 15$–20 μs, $W_0 \leqslant 3$ MJ). X-ray emission from both a discharge in pure neon and with a tungsten wire array placed on the axis of the discharge chamber was detected. The wire array imploded under the action of the electric current intercepted from the plasma current sheath of the PF discharge in neon. The measured soft X-ray powers from a conventional PF discharge in gas and a PF discharge in the presence of a wire array were compared for the first time.

DOI: 10.1134/S1063780X15110033

1. INTRODUCTION

At present, experiments on the implosion of current-carrying plasma loads, intended for the development of high-power soft X-ray (SXR) sources on the basis of Z-pinch, are being actively carried out worldwide. As a rule, megampere current generators are used for this purpose. Apparently, the first experiments with wire arrays were performed at the OWL II megampere facility [1]. Wire array loads are currently being used in the experiments carried out at modern electrophysical facilities, such as Z (United States); Angara-5-1, S-300, and EMG (Russia); MAGPIE (United Kingdom); and SPHINX (France) [2–7]. In the experiments performed at the Z facility at a current amplitude of 18 MA and current pulse duration of 100 ns, the implosion of tungsten wire arrays was accompanied by the generation of SXR pulses ($h\nu >$ 200 eV) with a duration of 5–8 ns, a power of 280–320 TW, and an energy of 1.8–2 MJ [3, 8]. The experiments carried out at the less powerful Angara-5-1 facility [2, 9, 10] demonstrated that, at currents of up to 4 MA, it is possible to obtain SXR pulses with a duration of about 6 ns, a power of 5–7 TW, and an energy of >30 kJ. It was shown that the physical mechanisms of wire array implosion at the most powerful ZR facility and other PF devices are similar [11] in spite of a considerable difference in their discharge currents.

At the same time, experiments the arrangement of which differs substantially from that in the above-cited works are also of considerable interest from the standpoint of understanding the physics of the load implosion and optimizing the design of plasma loads for future-generation high-power facilities, such as Baikal ($I \approx 50$ MA, $T/4 \approx 100$ ns). This concerns both the type of load (gas puffs of different configurations, their combinations with wire arrays, preliminarily prepared high-quality plasma current sheaths (PCSs), etc.) and the characteristic duration of the current pulse, which can reach 1 μs and more. The latter is of particular interest, because, at comparable currents, microsecond facilities are considerably simpler and cheaper than nanosecond ones. Thus, the implosion of a wire array under gas puff conditions was successfully achieved at the GIT-12 facility ($I \approx 2.6$ MA, $T/4 \approx$ 270 ns, Russia) [12].

The possibility of implosion of various loads, including wire arrays, in plasma focus (PF) devices was demonstrated in [13–16]. In recent years, experiments with tungsten wire arrays have been carried out at the PF-3 facility (Kurchatov Institute, Russia). It was shown [17] that the implosion of tungsten wires by the PCS of a PF discharge is accompanied by a number of phenomena inherent in the implosion of wire arrays at high-current accelerators with a nanosecond current rise time. Among these phenomena, there are extended plasma production from the load wires, the formation of a current precursor on the wire array axis before the arrival of the PCS and implosion of the bulk plasma, and the so-called "plasma rainstorm."

One of the key issues in studying the implosion of wire arrays is analysis of the power and spectrum of X-ray emission. Traditionally, the hard component of X-ray emission ($h\nu > 1$ keV) is measured in PF experiments. However, there are also works devoted to measurements of PF X-ray emission generated in the spectral range of 100–300 eV during PCS implosion [18, 19]. So far, no attempts were made to measure the power of SXR emission (20 eV < $h\nu$ < 500 eV) from imploding wire arrays at PF devices, because this emission is almost completely absorbed by the working gas under conditions of stationary filling of the discharge chamber. For the same reason, SXR emission is difficult to extract from the chamber for any practical use. Nevertheless, this difficulty can be overcome by placing the irradiated object in the immediate vicinity of the SXR source and, thereby, avoiding absorption of radiation by the working gas.

In this work, we present results of measurements of the SXR yield from both a PF discharge in pure neon and a PF discharge in the presence of a tungsten wire array on the axis of the discharge chamber. The idea of the experiment was to substantially reduce the absorption of X-ray emission in the working gas of the PF facility by creating a vacuum channel for radiation transportation from the source to the detector.

Taking into account the aforesaid, the goals of this work were as follows:

(i) to create a system for detecting X-ray emission in the spectral range from 6 eV to 1 keV;

(ii) to measure the emission characteristics of conventional PF discharges in gas and PF discharges in the presence of additional loads;

(iii) to study the interrelation between the formation dynamics of the emission source during the implosion of a wire array and the time dependence of the SXR power.

2. ARRANGEMENT OF THE EXPERIMENT

Experiments on the implosion of wire arrays under PF conditions were performed at the PF-3 Filippov-type facility ($I \leqslant 3$ MA, $T/4 \approx 15$–20 μs, $W_0 \leqslant 3$ MJ; see [14, 20] for details). The diameter of the glass ceramic insulator of the facility is 90 cm, and its height is 25 cm. The anode is a copper disk with a diameter of 92 cm and thickness of 2.5 cm. The total capacitance of the power supply is 9.2 mF, and the maximum charging voltage is 25 kV, which corresponds to a stored energy of 2.8 MJ.

To study the emission characteristics of the discharge, we created a system for detection of X-ray emission in the spectral range of up to 1 keV. The main requirement to the system for detection of X-ray emission from the wire array pinch was to reduce emission absorption by the working gas in the discharge chamber of the facility, as well as in the detection channel itself. To this end, the channel should have its own pumping-out system. The design of one of the detection channels is shown in Fig. 1a.

To reliably detect SXR emission in different spectral ranges, we manufactured two detection channels located on the upper lid of the chamber at an angle of 60° to the chamber axis (see Fig. 1b). At smaller angles, SXR detection can be distorted by ion and plasma fluxes accelerated in the axial direction. Each detection channel consists of two coaxial stainless tubes. The outer tube is joined to the working chamber of the PF-3 facility via a gate and serves as a vacuum lock for the inner tube. The 1320-mm-long inner movable tube, permanently pumped out to a pressure of $<10^{-2}$ Torr, can be moved into the working chamber of the facility. We note that, when the end of the tube approached the pinch to a distance of less than 100 mm, strong perturbations of the PCS dynamics were observed. Therefore, in these experiments, the end of the inner tube was not placed closer than 130 mm to the pinch. On the tube end facing the emission source, there was a slit with a width of 0.2–0.5 mm and length of 10 mm. To prevent the penetration of the working gas with a pressure of 2–4 Torr inside the inner tube, the slit was covered with a thin nitrocellulose (NC) film made of zapon lacquer ($C_6H_9O_7N$) with an areal density of 10–20 μg/cm^2.

The movable tube of the measuring channel was moved up to the required distance from the emission source immediately before the PF discharge, which made it possible to perform preliminary training discharges without damaging the NC film. During the PF discharge, the NC film was evaporated and the slit made of a 0.2-mm-thick copper foil was damaged. The integrity of the NC film was monitored by measuring the residual gas pressure in the vacuum channels. SXR emission was detected by a vacuum X-ray diode (XRD) with a nickel cathode placed at the opposite end of the inner tube. A set of diaphragms arranged inside the movable tube provided reliable collimation of X-ray emission from the imploding wire array.

The areal density of the separating NC film was 13–23 μg/cm^2. Its spectral transmission and the spectral transmission of the working gas (neon) are shown in Figs. 2b and 2a, respectively. Figure 2c shows the absolute spectral sensitivity of the XRD with allowance for the transmission of the NC film. The dependences of the mass absorption coefficients on the photon energy, $\mu(h\nu)$, are taken from [21, 22], and the quantum efficiency of the nickel cathode is taken from [23, 24].

The XRD spectral characteristics presented in Fig. 2 allow one to estimate the figure of merit of the measuring vacuum channel with the NC filter placed at a distance of 180 mm from the emission source as compared to emission measurements performed at a distance of 540 mm behind the standard gate. Even the threefold decrease in the path length of radiation

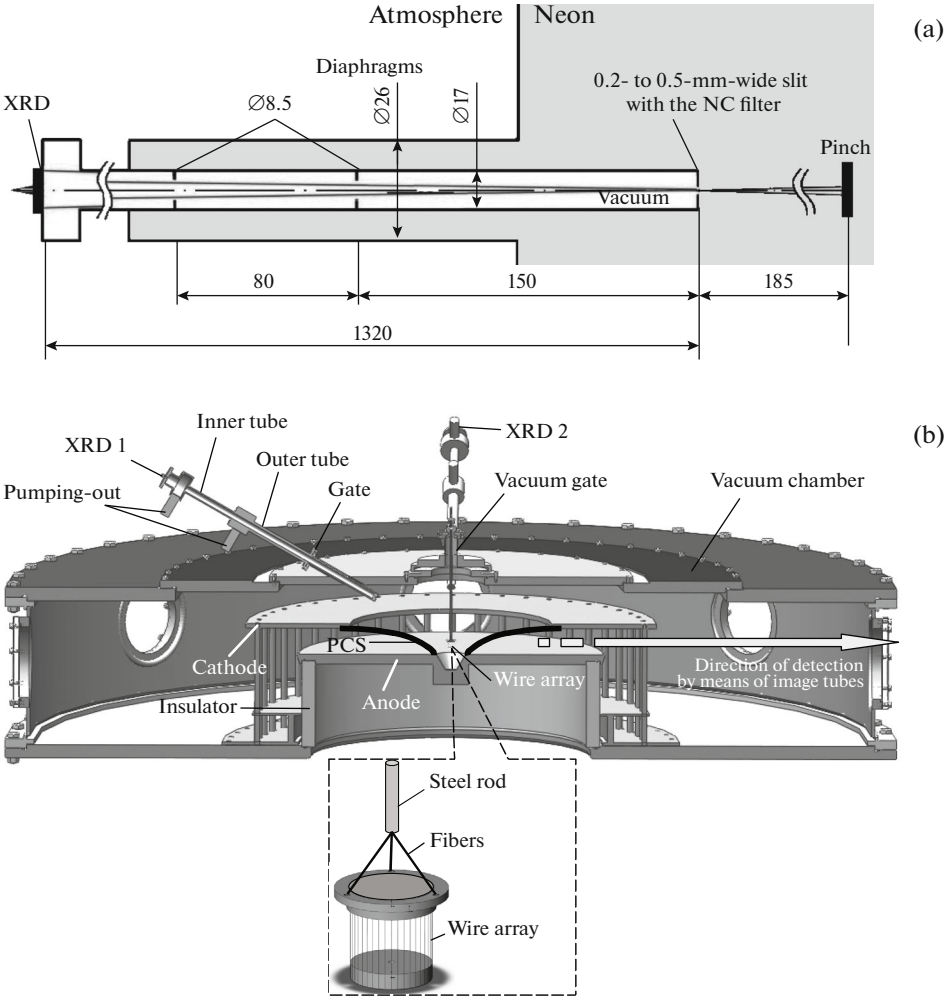

Fig. 1. System for detection of SXR emission ($h\nu < 1$ keV) at the PF-3 facility: (a) design of one of the two detection channels (all dimensions are in millimeters) and (b) schematic of the facility chamber and arrangement of the detection channels.

propagating through the working gas from the source to the detector leads to the 37-fold increase in the flux of 200-eV photons. The proposed system allows one to reliably detect SXR emission.

The slit of the measuring channel was oriented across the pinch axis (in a horizontal plane). Using this slit, the XRD with a diameter of the working cathode region of $D = 2$ cm was collimated onto a pinch segment with a height of 2–4 mm, depending on the distance between the slit and the plasma (see Fig. 3). The XRD anode was a thin perforated plate with a transparency of $T = 0.5$. A dc voltage of 400 V was supplied to the cathode. The XRD signals were recorded using a Tektronix TDS3034C oscilloscope with a transmission band of 300 MHz.

Let us estimate the light-gathering power Φ of the SXR detection channel (slit + XRD), the scheme of which is shown in Fig. 3. It depends on the solid angle Ω within which the radiation gets into the detector from each point of the pinch, $\Phi = (\Omega/4\pi)Tf_{cyl}(\theta)$, where $f_{cyl}(\theta)$ is the coefficient of radiation anisotropy for a cylindrical SXR source (further, it is assumed to be equal to unity), θ is the polar angle, and $T = 0.5$ is the transparency of the XRD anode grid (see Fig. 3). In our geometry, on the one hand, the slit is narrow in the sense that any point the emission source (pinch) yield a slit projection that entirely fits the height of the XRD cathode. On the other hand, the slit is sufficiently long for the total width of the XRD cathode be illuminated through this slit. It should be noted that, in our case, the XRD cathode was circular in shape; therefore, the width and height of the cathode were equal to its diameter D. Thus, considering the slit to be narrow and long, i.e., $\Delta\psi = d/a < D/(a + b)$ and $\Delta\varphi = D/(a + b) < L/a$, we have

$$\begin{aligned}\Omega = \pi/4\Delta\varphi\Delta\psi &= \xi(d/a)D/(a+b)\\ &= \xi d(D/a^2)/(1+\Gamma),\end{aligned} \quad (1)$$

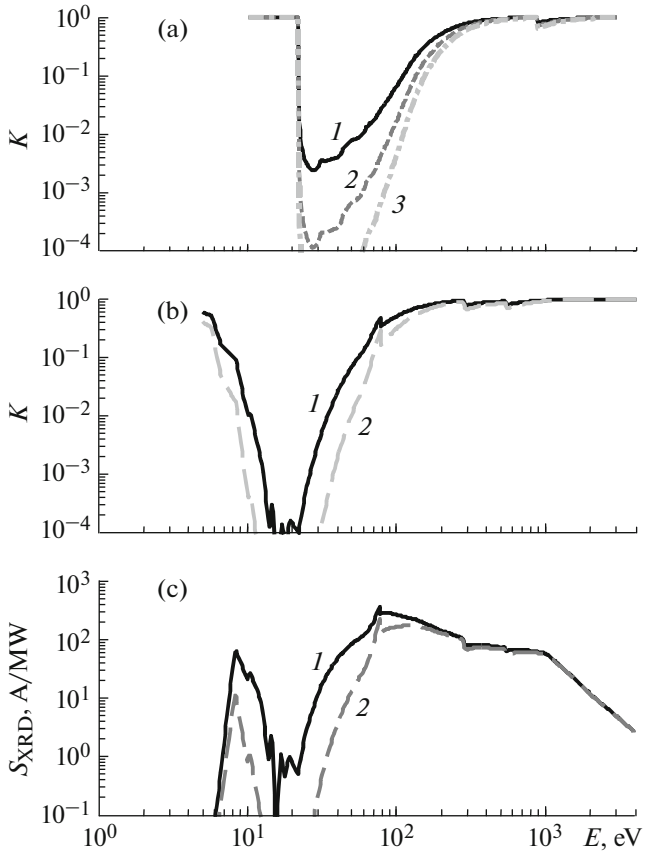

Fig. 2. (a) Spectral dependence of the transmission coefficient K of X-ray emission for neon at a = 10 cm and T = 295 K for (*1*) $\rho a = 22$ μg/cm^2 and a pressure of $P_0 = 2$ Torr, (*2*) $\rho a = 33$ μg/cm^2 and $P_0 = 3$ Torr, and (*3*) $\rho a = 44$ μg/cm^2 and $P_0 = 4$ Torr; (b) spectral dependences of the transmission coefficients of NC films with areal densities of (*1*) 13.5 and (*2*) 23 μg/cm^2; and (c) absolute sensitivities of XRDs with a nickel cathode and NC filters with the same values of the areal density as in panel (b).

where $\Delta\varphi$ is the azimuthal angle; $\xi = \pi/4$ is the coefficient accounting for the circular shape of the XRD input aperture when estimating $\Delta\varphi$; D is the cathode diameter; d is the slit width; a and b are the distances from the pinch to the slit and from the slit to the XRD, respectively; and $\Gamma = b/a$ is the magnification coefficient.

As is known, the final stage of the PF compression is characterized by an unpredictable displacement of the pinch with respect to the axis of the discharge chamber from shot to shot. This displacement can reach 10 mm, which created some difficulties for SXR measurements, because the viewing field of each SXR channel in the radial direction was 11 mm. As was noted above, the viewing field in the vertical direction was 3 mm. Two identical detection channels oriented in two mutually orthogonal azimuthal directions were used to measure SXR emission (see Fig. 1b). Both channels "saw" the same vertical segment of the pinch, which, under the natural assumption of the axial symmetry of pinch radiation, made it possible to perform comparative measurements. Due to the use of a standard KF vacuum junction and special holders, the channels preserved their observation directions after the regular disassembly and reassembly for the replacement of the filters covering the input slits after each PF discharge. The invariability of the observation direction was verified by two test adjustments performed in the course of the experiment, according to which the adjustment error in the vertical direction was about 1 mm. In view of the aforesaid, the signals measured using two SXR detection channels could be either identical in the shape and amplitude or differ substantially. As a rule, the maximum of the two XRD signals was used when processing the experimental data.

The SXR power and the parameters of the SXR spectrum are usually recovered from the recorded XRD signals by solving an ill-posed inverse problem, as it was done, e.g., in [25]. To enhance the accuracy of the recovery, the number of measurement channels in different spectral ranges should be as large as possible. Since, in our experiments, both detection channels were equipped with identical filters, the interpretation of the results of measurements of the radiation power included several variants corresponding to a prioi information on the emission spectrum. In experiments with wire arrays carried out at megam-

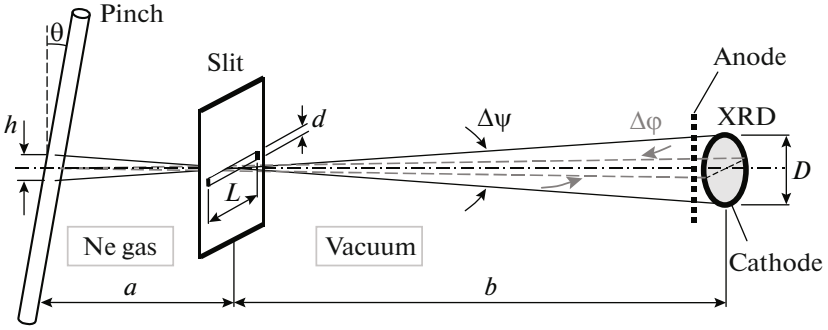

Fig. 3. Arrangement of the SXR source (pinch), spatial slit, and radiation detector (XRD).

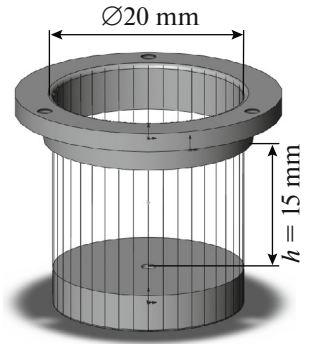

Fig. 4. General view of the wire array.

pere generators, it was found that most energy of the Z-pinch emission spectrum lies in the range from several eV to 500 eV. In this case, the XRD voltage measured using the oscilloscope is $U_{XRD}(t) = i(t)R = P_{SXR}(h\nu, t)\Phi K(h\nu)S_{XRD}(h\nu)R$, where R is the wave impedance of the cable (50 Ohm), $S_{XRD}(h\nu)$ is the absolute sensitivity of the XRD (in A/W) behind the filter, $i(t)$ is the XRD current (in A), and $P_{SXR}(h\nu, t)$ is the power of plasma radiation (in W). The expression for $U_{XRD}(t)$ also takes into account the spectral coefficient of radiation transmission through the working gas, $K(h\nu)$, between the source and the input slit of the XRD measuring channel according to the functions presented in Fig. 2.

Formula for calculating the radiation power per unit pinch height, $P(h\nu, t)$ (in W/cm), from the value of the oscilloscope voltage with allowance for the absorption in the working gas, the geometry of the measuring channel, and the absolute sensitivity of the XRD is as follows: $P(h\nu, t) = P_{SXR}(h\nu, t)/h = P_{SXR}(h\nu, t)\Gamma/D$, where $h = aD/b = D/\Gamma$ is the pinch height.

Substituting all necessary quantities into the expression for the linear power $P(h\nu, t)$, we finally obtain

$$P(h\nu,t) = 0.64\Gamma(1+\Gamma)\frac{a^2}{dD^2}\frac{U_{XRD}(t)}{S_{XRD}(h\nu)K(h\nu)}. \quad (2)$$

Table 1

Shot no.	Load in the axial region of the facility	Discharge parameters
4237	–	Ne gas $P_0 = 3.0$ Torr $U_0 = 10$ kV $W_0 = 460$ kJ
4238–4242	20-mm-diameter 15-mm-high wire array made of 40 6-μm-diameter tungsten wires with a total linear mass of 220 μg/cm	

In addition to the above SXR measurements, we used the following PF-3 standard diagnostics:

(i) measurements of the total discharge current by a Rogowski coil with an absolute sensitivity of 192 kA/V;

(ii) measurements of the time derivative of the total current by a loop probe with a sensitivity of 3×10^{10} A/(V s), located near one of the current buses of the facility collector;

(iii) measurements of radiation in the spectral range above 1 keV by using an RPPD-11 PIN diode covered with a 7-μm-thick aluminum foil with a time resolution better than 5 ns.

The process of wire array implosion was monitored by means of an optical streak camera and four frame electron-optical cameras. The frame exposure was 12 ns, the time interval between frames being 150 ns.

Tungsten wire arrays were used as plasma-forming loads. The array consisted of 40 6-μm-diameter tungsten wires arranged uniformly along the generatrix of a 20-mm-diameter cylinder rested on two coaxial cylindrical electrodes spaced by 15 mm (see Fig. 4). The wires were strained under the weight of the lower electrode. The linear mass of one tungsten wire was about 5.5 μg/cm. In the series of experiments described below, neon at an initial pressure of about 3 Torr was used as the working gas. The total energy W_0 stored in the capacitor bank at a charging voltage $U_0 = 10$ kV was 460 kJ. The parameters of the wire array and the gas discharge in the PF-3 chamber are given in Table 1. The wire array was suspended on a rod made of 12Kh18N10T nonmagnetic stainless steel. It was inserted through a vacuum gate into the axial region of the PCS final compression (see in Fig. 1) after a series of training discharges without violation of vacuum conditions in the chamber.

3. EXPERIMENTAL RESULTS

Figure 5 sows typical time dependences of the total current I and its time derivative dI/dt for the above parameters of a discharge in neon. The current rise time to the peak value of ~2 MA was about 15 μs. The PCS compression onto the axis and the formation of the PF pinch are accompanied by the appearance of a dip in the time dependence of the total current derivative dI/dt (see Fig. 5).

SXR emission in the photon energy range of <1 keV from discharges in neon without wire arrays was measured using two detection channels with input slits of width $d = 0.3$ mm and NC filters with an areal density of 23 μg/cm^2 (see Table 2). The inputs of both detection channels were placed at the same distance of $a =$ 13 cm from the emission source. Several tens of discharges in pure neon were performed.

Let us consider shot no. 4237, in which the maximum SXR power was achieved. The results in this shot are presented in Fig. 6 and Table 2. It follows from

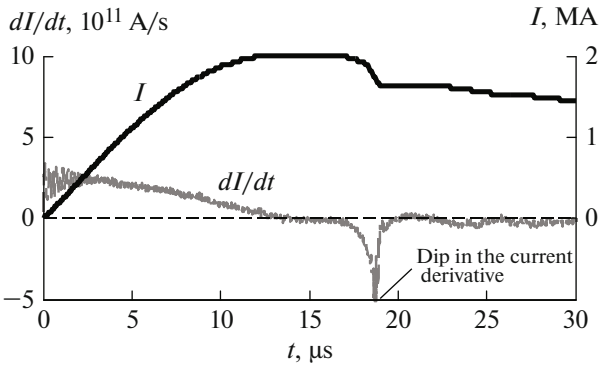

Fig. 5. Typical waveforms of the total current I and its time derivative dI/dt in discharges in neon at a pressure of P_0 = 3 Torr, U_0 = 10 kV, and W_0 = 460 kJ.

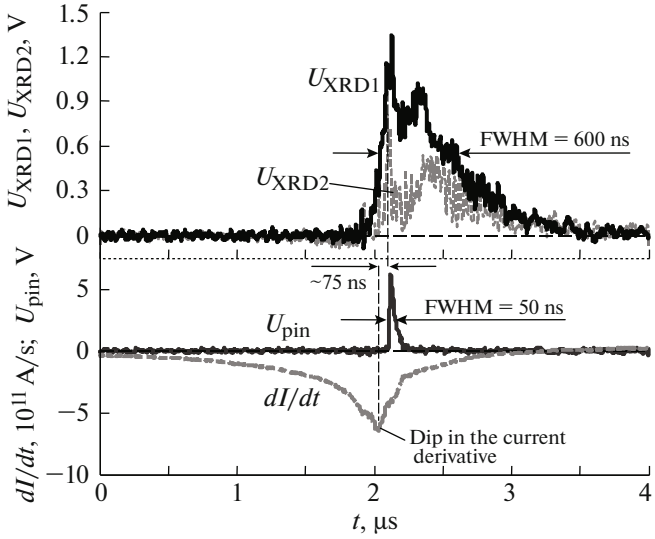

Fig. 6. X-ray signals measured by detectors XRD1 (U_{XRD1}) and XRD2 (U_{XRD2}) and the pin diode (U_{pin}) and waveform of the total current derivative dI/dt in shot no. 4237 without a wire array (Ne, P_0 = 3 Torr, U_0 = 10 kV, and W_0 = 460 kJ).

Fig. 6 that the SXR power begins to be recorded by detectors XRD1 (U_{XRD1}) and XRD2 (U_{XRD2}) at the time corresponding to the dip in the total current derivative dI/dt and reaches its maximum in about 75 ns. The profiles of the SXR pulses measured by detectors XRD1 and XRD2 are two-humped in shape. The first narrow peak coincides with the maximum of the PIN diode signal U_{pin}, which corresponds to X-ray emission with photon energies of $h\nu$ >1 keV. Since XRD-type detectors (unlike RPPD-11 ones) also detect SXR emission with photon energies of <1 keV, the trailing edges of their signals are substantially longer than the short trailing edge of the signal U_{pin}. The full width at the half-maximum (FWHM) of the SXR pulse measured by the XRD is about 600 ns, while the pin diode signal U_{pin} is considerably shorter (about 50 ns).

It was noted above that, since the system for detecting SXR emission with photon energies of <1 keV was in fact single-channel, the SXR power per unit pinch length was evaluated by formula (2) under assumption of emission monochromaticity for several variants with different values of the photon energy. When recovering the SXR power, radiation absorption in the working gas (neon) over a distance a from the SXR source to the input slit of the detection system (see Table 2) was taken into account. The emission energy was obtained from the recovered SXR power with allowance for the FWHM of the SXR pulse. The first variant in Table 2 concerns the first short peak (~50 ns) in the XRD1 signal, which coincides in time with the pin diode signal. Apparently, the main contribution to the first peak on the U_{XRD1} signal is made by photons with energies of $h\nu$ ~ 1 keV (the K shell of neon). In the second and third variants, it was assumed that the photon energies belong to the ranges corresponding to the L-shell emission of neon with photon energies of $h\nu$ = 150 and 200 eV, respectively. Apparently, it is emission with these photon energies that determines the ~600-ns duration of the XRD signal. The fourth variant corresponds to the lower boundary of the XRD sensitivity, which corresponds to photon energies of about 8–10 eV.

Under the above assumptions on the spectrum of the X-ray source, it follows from Table 2 that, in a discharge in neon without a wire array, the radiation power in the spectral range of $h\nu \leqslant 1$ keV was 2.5–9 GW/cm. The corresponding SXR energy was in the range from 0.16 to 5.4 kJ/cm.

Below, we consider results of experiments with wire arrays.

Figure 7 shows the main stages of PCS compression and wire array implosion recorded using an electron-optical frame camera in several discharges (shot nos. 4238–4242) with the same initial conditions (see Table 1). In the final stage of compression, the PCS approaches the location of the wire array (time t_1). As was shown in [17], during the interaction of the PCS with the wire array, the current is almost entirely switched to the wires. Within the time interval from t_2 to t_3, required for the entire wire material to be transformed into plasma (the phenomenon of extended plasma production [10]), a plasma precursor forms on the axis of the wire array. In the time interval from t_4 to t_6, when plasma production from the array wires had already terminated, the stage of the final plasma compression and the formation of a Z-pinch with a diameter of 1.5–3 mm and height of 8–10 mm begins. A certain amount of the wire material that remains after termination of plasma production from the array wires and is not compressed onto the array axis (the so-called trailing mass, see frame t_4) is present at the

Table 2

Shot no.	Distance a from the pinch to the slit and slit width d, cm	NC filter, μg/cm^2	Signal amplitude,* V; signal FWHM, ns	Photon energy $h\nu$, eV	SXR power** P_{max}, GW/cm	SXR energy** W_{max}, kJ/cm
4237	13/0.03	23.0	~1.2/50	1000	3.3	0.16
			0.9/600	200	2.5	1.5
			0.9/600	150	5.9	3.5
			0.9/600	8	9.0	5.4

* With allowance for the 1 : 1.5 divider.** With allowance for absorption in the working gas.

periphery of the wire array The main stages of the implosion of a wire array and the compression dynamics of its plasma were discussed in detail in [17].

Let us compare the compression dynamics of the wire array plasma obtained using the electron-optical frame camera with the results of time-resolved SXR measurements by means of XRDs.

First, we consider shot no. 4241. In the optical frame images corresponding to this shot (see Fig. 8), the dynamics of the wire array until the beginning of the stage of final compression are illustrated. In the frame taken at the time t_1 (250 ns before the dip in the total current derivative dI/dt), one can see the PCS approaching the wire array. The location of the wire array is shown by the dashed rectangle. In the frame taken at the time t_2, the PCS has already begun to interact with the wire array. One can see that PCS compression is somewhat asymmetric with respect to the wire array. Before this time, diode XRD2 does not detect radiation from the wire array. At the time t_3, a small pedestal is observed in the signal U_{XRD2}, which is associated with the X-ray emission of the plasma precursor on the wire array axis, as is seen in the corresponding optical frame image. At the periphery of the wire array (at the initial array radius), there is the remaining wire material from which the plasma continues to be produced. After the termination of plasma production from the wires, the stage of final plasma compression onto the array axis begins (see the frame corresponding to the time t_4). The maximum of the SXR power in the signal U_{XRD2} is reached ≈500 ns after the dip in the total current derivative. The FWHM of the SXR pulse in this case is about 880 ns.

It should be noted that the interaction of the PCS with the wire array improves the location of compressed plasma on the axis of the chamber as compared to conventional discharges in neon.

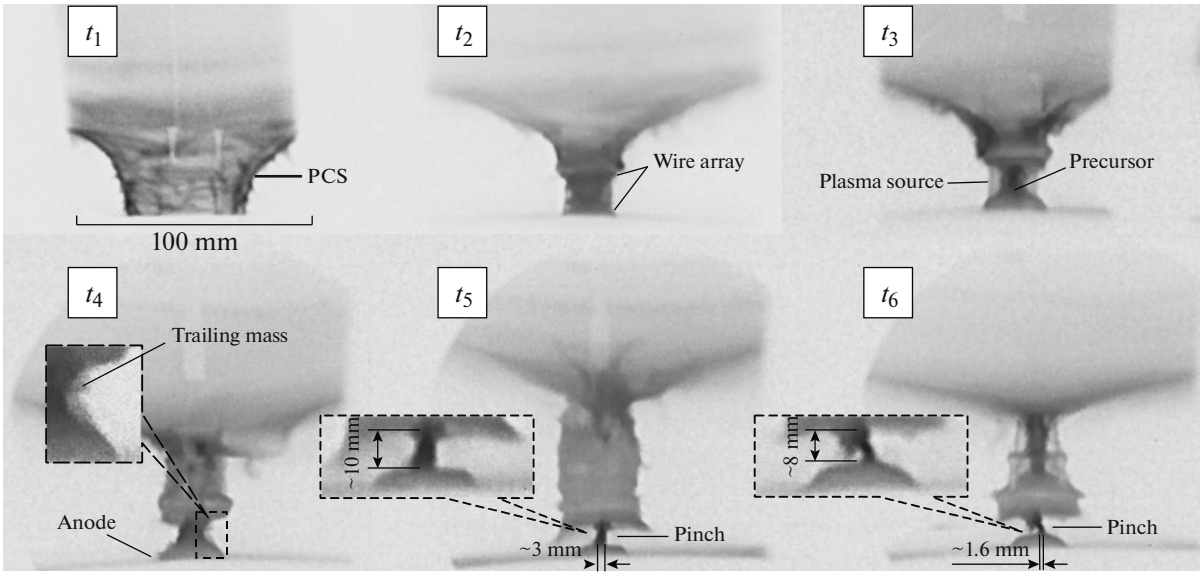

Fig. 7. Implosion of the CPS and wire array according to data from optical frame images taken in shot nos. 4238–4242. The 20-mm-diameter 15-mm-high wire array consists of 40 6-μm-diameter tungsten wires with a total linear mass of 220 μg/cm. The surface of the facility anode is on the bottom.

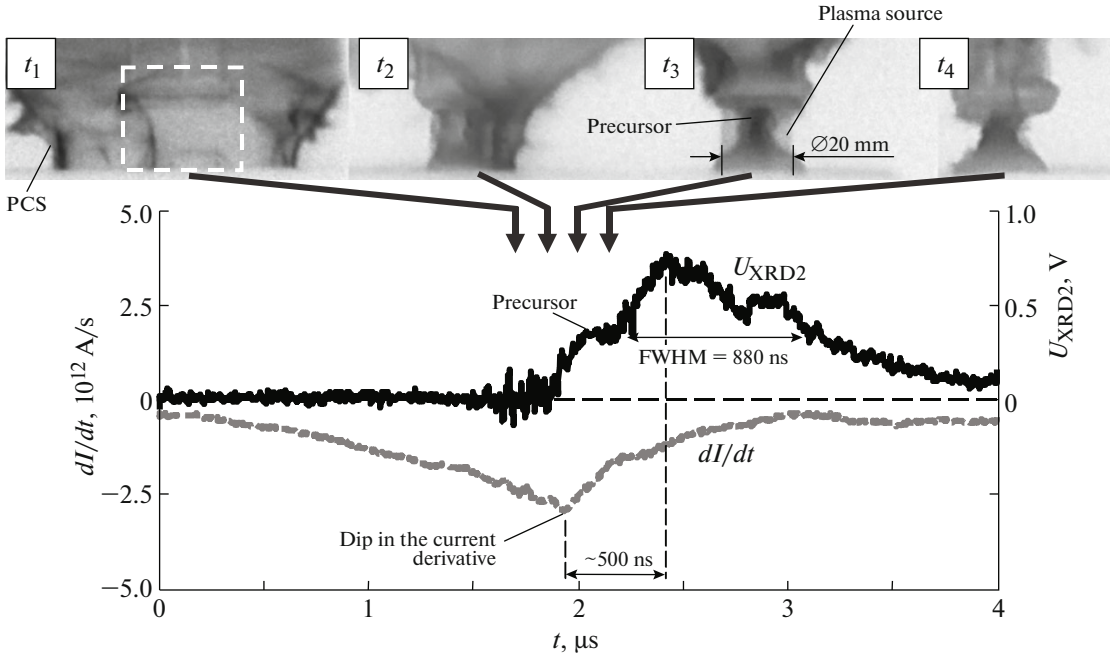

Fig. 8. Waveforms of the total current derivative dI/dt and X-ray intensity measured by detector XRD2 (U_{XRD2}) in a PF discharge in neon in the presence of a 20-mm-diameter 15-mm-high wire array consisting of 40 6-μm-diameter tungsten wires with a total linear mass of 220 μg/cm (shot no. 4241, $P_0 = 3$ Torr, $U_0 = 10$ kV, and $W_0 = 460$ kJ). On top: optical frame images synchronized with the above waveforms. The times $t_1 = -250$ ns, $t_2 = -100$ ns, $t_3 = +50$ ns, and $t_4 = +200$ ns are counted from the instant corresponding to the dip in the waveform of dI/dt. The location of the wire array is shown by the dashed rectangle.

The region occupied by the compressed Z-pinch plasma (see optical frames Fig. 7) on the wire array axis is 8–10 mm in height, which is substantially shorter than the wire array height (15 mm). The positions of the XRDs and the wire array were adjusted in such a way that the XRD fields of view coincided with the region of Z-pinch compression or was somewhat lower. When the XRDs saw the lower part of the Z-pinch, the signals from them were lower in amplitude and had a longer duration (see Fig. 8). When the XRD fields of view got in the compactly compressed middle part of the Z-pinch, the signals were larger in amplitude and had a shorter duration. It is this case that will be considered below in more detail.

Figure 9 and Table 3 show the results of measurements of the SXR power from the wire array Z-pinch in shot no. 4242, in which the final stage of wire array implosion and the formation of the Z-pinch were observed in optical frame images. As in shot no. 4241, the XRD signal U_{XRD1} begins to be detected at the time close to the dip in the current derivative dI/dt. At the time t_1, the precursor is observed inside the wire array and a pedestal is present in the XRD1 signal. At the time t_2, the process of plasma production from the wires has already terminated and the stage of final plasma compression has begun. In the stage of final compression of the wire array plasma, the XRD signal increases and reaches its peak value at 500 ns after the dip in the total current derivative. At the time corresponding to the maximum of the SXR power, the formed pinch is observed on the wire array axis (see optical frames taken at the times t_3 and t_4). The FWHM of the SXR pulse in this shot was about 650 ns, which is about 1.4 times shorter than for shot no. 4241.

It should be noted that, in the presence of a wire array in the PF discharge, the signal from the pin diode, which detects radiation in the spectral range above 1 keV, was absent. Apparently, this is due to the softening of the emission spectrum of the pinch produced from the tungsten wire array as compared to that of the neon PCS. It is reasonable to consider that, in this case, photons with energies of >1 keV also did not contribute to the U_{XRD1} signal. The results of the recovery of the SXR power and SXR energy from XRD signals are presented in Table 3 for the same photon energies as in Table 2 (8, 150, and 200 eV).

Comparison of the results presented in Tables 2 and 3 shows that, in the presence of a tungsten wire array in the region of PCS final compression, the power of X-ray emission in the spectral range of 100–200 eV is at least three to four times higher than during the compression of a neon PCS. For the same level of the discharge current as in experiments with a neon PCS, the estimated linear power and energy of SXR emission ($h\nu < 1$ keV) vary in the ranges of 6–20 GW/cm and 4–13 kJ/cm, respectively, depending on the supposed radiation spectrum of the Z-pinch wire array.

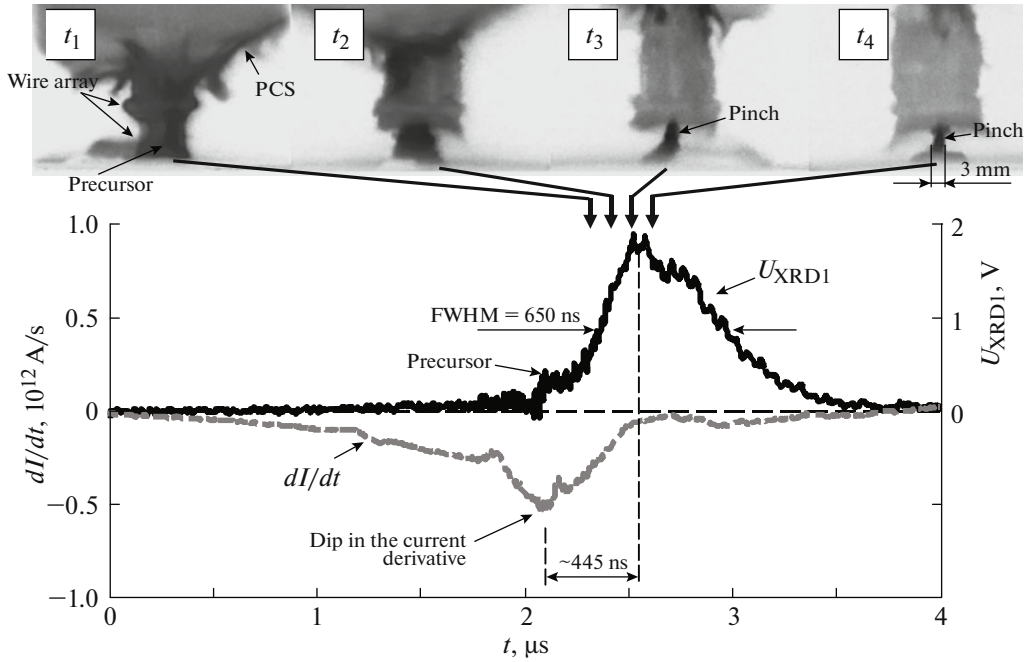

Fig. 9. Waveforms of the total current derivative dI/dt and X-ray intensity measured by detector XRD1 (U_{XRD1}) in a PF discharge in neon in the presence of a 20-mm-diameter 15-mm-high wire array consisting of 40 6-μm-diameter tungsten wires with a total linear mass of 220 μg/cm (shot no. 4242, $P_0 = 3$ Torr, $U_0 = 10$ kV, and $W_0 = 460$ kJ). On top: optical frame images synchronized with the above waveforms. The times $t_1 = +80$ ns, $t_2 = +230$ ns, $t_3 = +380$ ns, and $t_4 = +530$ ns are counted from the instant corresponding to the dip in the waveform of dI/dt.

4. DISCUSSION OF RESULTS

In experiments with wire arrays performed at the PF-3 facility, the achieved level of the radiation energy (4–13 kJ/cm) in the spectral range of $h\nu < 1$ keV is close to that observed in experiments on the implosion of wire arrays carried out at the same level of the discharge current at high-power electrophysical facilities with nanosecond-range current pulse durations, such as COBRA (1 MA, 100–150 ns, Cornell University, United States), ZEBRA (1 MA, 80–100 ns, College of Science University of Nevada, United States), and MAGPIE (1–1.4 MA, 240 ns, Imperial College, United Kingdom) [26–29]. However, the SXR power (6–20 GW/cm) in the same spectral range was substantially lower than the power of 200–500 GW/cm achieved at the above facilities.

Experiments with gas puffs and wire arrays have shown that one of the possible reasons for the limitation of the radiation power can be that the fraction of the total current switched from the gas puff to the wire array is too small, due to which the compression dynamics of the Z-pinch is violated. For example, the experiments carried out at the GIT-12 facility [12] showed that the current from gas puff PCS could be switched to the wire array only when the total impedance of the gas puff plasma was higher than the impedance of the wire array, i.e., the condition $R_{gas} + dL_{gas}/dt > R_{wa}$ was satisfied. The wire array impedance R_{wa} is inversely proportional to the number of wires in

Table 3

Shot no.	Distance a from the pinch to the slit and slit width d, cm	NC filter, μg/cm^2	Signal amplitude,* V; signal FWHM, ns	Photon energy $h\nu$, eV	SXR power** P_{max}, GW/cm	SXR energy** W_{max}, kJ/cm
4242	18.5/0.045	23.0	1.8/650	200	5.6	3.6
				150	20	13.0
				8	12.6	8.2

* With allowance for the 1 : 1.5 divider.

** With allowance for absorption in the working gas.

the array; therefore, the efficiency of current switching from the gas puff PCS should increase with increasing number of wires in the array. The experiments carried out at the Angara-5-1, C-300, and MAGPIE facilities have shown that the current cannot be entirely switched to the wire array. A fraction of the current-carrying plasma penetrates inside the wire array, due to which the efficiency of tungsten plasma compression in the final stage of implosion is reduced. It was shown experimentally that this fraction of the current can be substantially reduced by increasing the number of wires in the array [30–32].

The growth rate of the current flowing through the array wires during current switching depends on the PCS compression velocity V_r and the PCS thickness δ_{PCS} as the instant of its interaction with the wire array, $dI/dt \approx (V_r/\delta_{PCS})I$. For a current at a level of 1–1.5 MA, the PCS propagation velocity of $(0.5–1) \times 10^7$ cm/s, and the PCS thickness of about 1 cm, the growth rate of the current flowing through the array wire is $(0.5–1.5) \times 10^{13}$ A/s and the current rise time to the peak value is 100–200 ns, which is comparable with the implosion time of wire arrays in experiments carried out at high-power electrophysical facilities with nanosecond-range current pulse durations. The experiments performed at the PF-3 facility show that, when the above condition is satisfied, the current is almost entirely switched from the PCS to the wire array and almost the entire wire array mass (about 80%) is compressed onto the axis [17].

The formation and heating of the pinch are associated, in particular, with the conversion of the kinetic energy of the counter-propagating plasma flows moving under the action of the Ampère force from the initial position of the exploded wires. The X-ray power P_{kin} generated due to the conversion of the kinetic energy of the wire array plasma into the internal energy of the Z-pinch can be estimated as follows:

$$P_{kin} = 5 \times 10^{-23} m V_r^3 / \Delta_r, \quad (3)$$

where P_{kin} is in GW/cm, Δ_r is the thickness of the wire array plasma (in cm), V_r is its compression velocity (in cm/s), and m is its linear mass (in μg/cm).

For the experimentally observed compression velocity of the wire array plasma of about 5×10^6 cm/s and the plasma thickness of 0.2–0.3 cm (see [17]), we obtain $P_{kin} \sim 5–10$ GW/cm. In the zero-dimensional model (see [33]), the expression for the radial compression velocity V_r of the wire array plasma with allowance for the number of wires has the form

$$|V_r(t)| = 10^6 \frac{N-1}{N} \frac{1}{m} \int \frac{I^2(t)}{r(t)} dt, \quad (4)$$

where I is the current (in MA), r is the plasma radius (in cm), and N is the number of wires in the array. It should be noted that, for a sufficiently large number of wires, we have $(N-1)/N \to 1$. The numerical calculation by formula (4) shows that, in order to achieve the experimentally observed compression velocity of the wire array of 5×10^6 cm/s, it is necessary that the current switched to the array be no less than 1 MA. Thus, X-ray measurements indirectly confirm the results of [17], according to which the current is efficiently switched from the PCS to the wire array.

Another reason for the limitation of the SXR power generated by the Z-pinch is that a fraction of the plasma remains at the periphery of the wire array (at the initial position of the wires) [34]. This occurs in the final stage of plasma compression, when plasma production at the periphery of the wire array has already terminated. If there still remains plasma in this region of the wire array, then it can shunt a fraction of the discharge current. This should lead to a decrease in the electromagnetic power delivered into the axial region. As a result, the compactness of the Z-pinch compression deteriorates and, accordingly, the SXR power is reduced. In this case, a fraction of the electromagnetic power of the facility generator is lost due to the current leakage at the periphery of the wire array. It should be noted that Z-pinch compression is a consequence of the breakthrough of the magnetic flux and plasma inside the wire array. In the course of its formation, the pinch is heated due to both the conversion of the kinetic energy of the counter-propagating plasma flows formed under the action of the Ampère force and the absorption of the magnetic field energy supplied from the discharge circuit. The phenomenon of the breakthrough of the magnetic flux inside the wire array in the final stage of plasma production was studied experimentally in [35, 36].

Analysis of the physical mechanisms governing the conversion of the electromagnetic energy of the discharge into the plasma thermal energy in the stage of final compression requires further experimental studies and goes beyond the scope of the present work. It is worth noting, however, that, according to the theoretic model proposed in [37–39], the electromagnetic energy of the discharge circuit can be converted into the internal energy of the Z-pinch due to MHD turbulent mixing of the plasma and the magnetic flux penetrating into the Z-pinch with a velocity close to the Alfvén velocity and may further be spent on the generation of the SXR pulse. Using the expression for the SXR power obtained in [37–39], we obtain the following estimate for the linear SXR power P_{MHD} (in units of GW/cm) generated due to such MHD mixing:

$$P_{MHD} = \frac{B_\varphi^2}{8\pi} 2\pi r V_A \approx 500 \frac{I^3}{r_{pinch}\sqrt{m}}, \quad (5)$$

where I is the current (in MA) flowing through the Z-pinch with a radius r_{pinch} (in mm) and linear mass m (in μg/cm). For the experiment values $I = 1$ MA, $r_{pinch} = 1.5–3$ mm, and $m = 220$ μg/cm, we find that P_{MHD} is about 10–20 GW/cm.

It should be noted that, since P_{MHD} depends strongly on the pinch current and pinch radius, it is necessary to have detailed information on the radial distribution of the current inside the wire array, which was unavailable in the present experiments. Therefore, the above estimate of the SXR power is only qualitative in character. Nevertheless, the values of P_{kin} and P_{MHD} estimated from expressions (3) and (5) are comparable with the measured level of the linear SXR power. According to expression (4), in order for the compression velocity of the wire array plasma V_r in the final stage of implosion to increase twofold (i.e., to 10^7 cm/s), it is necessary that the amplitude of the discharge current also increases twofold, provided that the time dependence of the current $I(t)$ and the linear mass of the wire array remain the same. In this case, according to formulas (3) and (5), the values of P_{kin} and P_{MHD} will increase nearly by one order of magnitude. An increase in P_{kin} can also be achieved by optimizing the parameters of the wire array, e.g., its linear mass and initial radius. The optimization of the wire array design also implies an increase in the array height. Indeed, it follows from the optical frames in Figs. 7 and 9 that, when the PCS approaches the wire array, its height is about a factor of 1.5–2 larger than the height of the wire array (15 mm). The electrotechnical measurements show [20] that, when the PCS is compressed onto the axis, the inductance of the discharge reaches a value of about 100–130 nH, which is substantially larger than the self-inductance of the imploding wire array (about 7 nH). Thus, the increase in the initial inductance of the wire array due to the two- to threefold increase in its height should not decrease the discharge current in the final stage of PCS compression and, consequently, should not deteriorate the implosion process. In this case, the height of the radiating pinch region and, accordingly, the total SXR will increase in proportion to the increase in the wire array height.

Thus, the twofold increase in the discharge current and the optimization of the wire array design makes it possible, in principle, to increase P_{MHD} nearly by one order of magnitude and reach an SXR power of 200–500 GW/cm, previously achieved at nanosecond-range "vacuum" generators with the same level of the discharge current. Nevertheless, there is a series of effects that may limit the radiation power.

(i) The counter-pressure produced on the "tungsten" plasma by the high-energy low-emissive material of the neon PCS, which penetrates through the wire array and possesses a larger time of ion-to-electron energy transfer.

(ii) The heating of the "inner" plasma by the current of the precursor penetrating inside the array in the stage of plasma production from the array wires.

(iii) The absence of dissipation of the electromagnetic energy (or its substantial reduction) due to MHD turbulence in the stagnation stage caused by the shunting of the Z-pinch current by the rarefied peripheral plasma and the residual gas.

(iv) An increase in the duration of the X-ray pulse due to the so-called "zipper" effect, which occurs due to oblique propagation of the PCS front with respect to the axis and leads to the nonsimultaneous plasma compression over the Z-pinch height.

To study the influence of these effects and find ways to overcome them will be a natural continuation of this experimental work.

5. CONCLUSIONS

A technique for detecting SXR emission in the spectral range from 20 eV to 1 keV has been elaborated, and comparative measurements of the SXR power from conventional PF discharges in neon and PF discharges in the presence of a tungsten wire array have been performed for the first time.

The obtained results allow us to draw the following conclusions.

(i) As follows from the electron-optical frame images of the imploding plasma, the maximum compression is achieved in the center of the wire array. The instant of the maximum compression corresponds to the peak of the SXR power ($h\nu < 1$ keV). For the total array height of 15 mm, the diameter of the Z-pinch is 1.5–3 mm and its height is 8–10 mm. The formation of the plasma precursor on the wire array axis correlates with the time dependence of the X-ray power. This process corresponds to the pedestal in the time profile of the SXR power.

(ii) It has been demonstrated for the first time that, in the presence of a tungsten wire array in a PF discharge, the power and energy of X-ray emission in the spectral range from 100 eV to 1 keV increases at least three- to fourfold as compared to the compression of a conventional neon PCS.

(iii) Estimates obtained under the assumption of the monochromaticity of SXR emission for different values of the photon energy (8, 150, 200, and 1000 eV) show that, at a discharge current of 1 MA, the linear SXR power and energy ($h\nu < 1$ keV) generated by the wire array Z-pinch amount to 6–20 GW/cm and 4–13 kJ/cm, respectively.

The SXR power can be increased by one order of magnitude (to about 0.5 TW/cm) by increasing the amplitude of the discharge current about twofold and optimizing the wire array parameters.

ACKNOWLEDGMENTS

This work was supported in part by the Russian Foundation for Basic Research (project nos. 11-02-01212, 14-02-00179, and 14-29-06085).

REFERENCES

1. C. Stalling, K. Nielsen, and R. Schneider, Appl. Phys. Lett. **29**, 404 (1976).
2. M. B. Bekhtev, V. D. Vikharev, S. V. Zakharov, V. P. Smirnov, M. V. Tulupov, and V. Ya. Tsarfin, Sov. Phys. JETP **68**, 955 (1989).
3. R. B. Spielman, C. Deeney, G. A. Chandler, M. R. Douglas, D. L. Fehl, M. K. Matzen, D. H. McDaniel, T. J. Nash, J. L. Porter, T. W. L. Sanford, J. F. Seamen, W. A. Stygar, K. W. Struve, S. P. Breeze, J. S. McGurn, et al., Phys. Plasmas **5**, 2105 (1998).
4. J. H. Hammer, M. Tabak, S. C. Wilks, J. D. Lindl, D. S. Bailey, P. W. Rambo, A. Toor, and G. B. Zimmerman, Phys. Plasmas **6**, 2129 (1999).
5. Yu. G. Kalinin, A. S. Kingsep, V. P. Smirnov, Yu. L. Bakshaev, A. V. Bartov, P. I. Blinov, S. A. Dan'ko, L. G. Dubas, A. V. Korel'skii, V. D. Korolev, V. I. Mizhiritskii, G. I. Ustroev, A. S. Chernenko, R. V. Chikin, A. Yu. Shashkov, et al., Plasma Phys. Rep. **32**, 656 (2006).
6. V. D. Selemir, V. A. Demidov, V. F. Ermolovich, V. F. Ermolovich, G. M. Spirov, P. B. Repin, I. V. Pikulin, A. A. Volkov, A. P. Orlov, A. S. Boriskin, O. M. Tatsenko, A. N. Moiseenko, M. A. Barinov, I. M. Markevtsev, S. A. Kazakov, et al., Fiz. Plazmy **33** (5), 424 (2007).
7. H. Calamy, F. Lassalle, A. Loyen, F. Zucchini, J. P. Chittenden, F. Hamann, P. Maury, A. Georges, J. P. Bedoch, and A. Morell, Phys. Plasmas **15**, 012701 (2008).
8. M. C. Jones, D. J. Ampleford, M. E. Cuneo, R. Hohlfelder, C. A. Jennings, D. W. Johnson, B. Jones, M. R. Lopez, J. MacArthur, J. A. Mills, T. Preston, G. A. Rochau, M. Savage, D. Spencer, D. B. Sinars, et al., Rev. Sci. Instrum. **85**, 083501 (2014).
9. E. V. Grabovski, G. M. Oleinik, and I. Yu. Porofeev, Plasma Phys. Rep. **32**, 475 (2006).
10. V. V. Aleksandrov, A. V. Branitsky, G. S. Volkov, E. V. Grabovski, M. V. Zurin, S. L. Nedoseev, G. M. Oleinik, A. A. Samokhin, P. V. Sasorov, V. P. Smirnov, M. V. Fedulov, and I. N. Frolov, Plasma Phys. Rep. **27**, 89 (2001).
11. S. V. Lebedev, F. N. Beg, S. N. Bland, J. P. Chittenden, A. E. Dangor, M. G. Haines, K. H. Kwek, S. A. Pikuz, and T. A. Shelkovenko, Phys. Plasmas **8**, 3734 (2001).
12. R. B. Baksht, A. Yu. Labetskii, A. G. Russkikh, A. V. Fedyunin, A. V. Shishlov, V. A. Kokshenev, N. E. Kurmaev, and F. I. Fursov, Plasma Phys. Rep. **27**, 557 (2001).
13. M. Scholz, L. Karpinski, W. Stepniewski, A. V. Branitski, M. V. Fedulov, S. F. Medovschikov, S. L. Nedoseev, V. P. Smirnov, M. V. Zurin, and A. Szydlowski, Phys. Lett. A **262**, 453 (1999).
14. V. E. Fortov, M. A. Karakin, E. Yu. Khautiev, V. I. Krauz, S. F. Medovschikov, A. N. Mokeev, V. V. Myalton, S. L. Nedoseev, V. P. Smirnov, and V. P. Vinogradov, in *Proceedings of the 5th International Conference on Dense Z-Pinches, Albuquerque, NM, 2002,* AIP Conf. Proc. **651**, 37 (2002).
15. M. A. Karakin, E. Yu. Khautiev, V. I. Krauz, A. N. Mokeev, D. Mourenas, V. V. Myalton, F. Simonet, V. P. Smirnov, V. P. Tykshaev, J. Vierne, V. V. Vikhrev, and V. P. Vinogradov, in *Proceedings of the 15th International Conference on High-Power Particle Beams, St. Petersburg, 2004,* p. 738.
16. V. I. Krauz, Plasma Phys. Controlled Fusion **48**, B221 (2006).
17. K. N. Mitrofanov, V. I. Krauz, V. V. Myalton, V. P. Vinogradov, Yu. V. Vinogradova, E. V. Grabovskii, S. A. Dan'ko, A. A. Zelenin, S. F. Medovshchikov, and A. N. Mokeev, Plasma Phys. Rep. **40**, 110 (2014).
18. V. I. Krauz, V. V. Myalton, and V. P. Vinogradov, Probl. At. Sci. Technol., Ser. Plasma Phys, No. 1, 98 (2003).
19. M. A. Karakin, E. Yu. Khautiev, V. I. Krauz, A. N. Mokeev, V. V. Myalton, V. P. Smirnov, V. P. Tykshaev, V. V. Vikhrev, V. P. Vinogradov, V. Ya. Nikulin, A. V. Oginov, D. Mourenas, and F. Simonet, in *Proceedings of the International Conference "Research and Applications of Plasma" (PLASMA-2003), Warsaw, 2003,* p. I3-3.
20. K. N. Mitrofanov, V. I. Krauz, E. V. Grabovski, V. V. Myalton, V. P. Vinogradov, M. Paduch, M. Shol'ts, and L. Karpiński, Plasma Phys. Rep. **41**, 379 (2015).
21. W. M. J. Veigele, At. Data Tables **54**, 51 (1973).
22. http://henke.lbl.gov/optical_constants/filter2.html
23. R. H. Day, P. Lee, E. B. Saloman, and D. J. Nagel, J. Appl. Phys. **52**, 6965 (1981).
24. H. E. Hinteregger and K. Watanabe, J. Opt. Soc. Am. **43**, 604 (1953).
25. A. V. Branitskii and G. M. Oleinik, Instrum. Exp. Tech. **43**, 486 (2000).
26. V. L. Kantsyrev, D. A. Fedin, A. A. Esaulov, A. S. Safronova, V. Nalajala, K. Williamson, G. Osborne, M. F. Yilmaz, N. D. Ouart, J. B. Greenly, J. D. Douglass, R. D. McBride, L. M. Maxson, D. A. Hammer, and A. L. Velikovich, IEEE Trans.Plasma Sci. **34**, 2288 (2006).
27. V. V. Ivanov, V. I. Sotnikov, J. M. Kindel, P. Hakel, R. C. Mancini, A. L. Astanovitskiy, A. Haboub, S. D. Altemara, A. P. Shevelko, E. D. Kazakov, and P. Sasorov, Phys. Rev. E **79**, 056404 (2009).
28. S. V. Lebedev, D. J. Ampleford, S. N. Bland, S. C. Bott, J. P. Chittenden, J. Goyer, C. Jennings, M. G. Haines, G. N. Hall, D. A. Hammer, J. B. A. Palmer, S. A. Pikuz, T. A. Shelkovenko, and T. Christoudias, Plasma Phys. Controlled Fusion **47**, A91 (2005).
29. S. N. Bland, S. V. Lebedev, J. P. Chittenden, G. N. Hall, F. Suzuki-Vidal, D. J. Ampleford, S. C. Bott, J. B. A. Palmer, S. A. Pikuz, and T. A. Shelkovenko, Phys. Plasmas **14**, 056315 (2007).
30. A. S. Chernenko, V. P. Smirnov, A. S. Kingsep, Yu. G. Kalinin, Li Zhenghong, H. Xinsheng, Yu. L. Bakshaev, A. V. Bartov, P. I. Blinov, R. V. Chikin, S. A. Dan'ko, L. G. Dubas, A. V. Korel'sky, V. D. Korolev, E. V. Kravchenko, et al., in *Proceedings of the 14th IEEE International Pulsed Power Conference, Dallas, TX, 2003,* Vol. 2, p. 863.
31. S. N. Bland, S. V. Lebedev, J. P. Chittenden, C. Jennings, and M. G. Haines, Phys. Plasmas **10**, 1100 (2003).
32. E. V. Grabovski, G. G. Zukakishvili, K. N. Mitrofanov, G. M. Oleinik, I. N. Frolov, and P. V. Sasorov, Plasma Phys. Rep. **32**, 32 (2006).

33. F. S. Felber and N. Rostoker, Phys. Fluids **24**, 1049 (1981).

34. M. E. Cuneo, E. M. Waisman, S. V. Lebedev, J. P. Chittenden, W. A. Stygar, G. A. Chandler, R. A. Vesey, E. P. Yu, T. J. Nash, D. E. Bliss, G. S. Sarkisov, T. C. Wagoner, G. R. Bennett, D. B. Sinars, J. L. Porter, et al., Phys. Rev. E **71**, 046406 (2005).

35. K. N. Mitrofanov, V. V. Aleksandrov, E. V. Grabovskii, E. A. Ptichkina, A. N. Gritsuk, G. M. Oleinik, I. N. Frolov, and Ya. N. Laukhin, Plasma Phys. Rep. **40**, 679 (2014).

36. V. V. Ivanov, V. I. Sotnikov, G. S. Sarkisov, T. E. Cowan, S. N. Bland, B. Jones, C. A. Coverdale, C. Deeney, P. J. Laca, A. L. Astanovitskiy, and A. Haboub, Phys. Rev. Lett. **97**, 125001 (2006).

37. R. H. Lovberg, R. A. Raily, and J. S. Shlachter, in *Proceedings of the 3rd International Conference on Dense Z-Pinches, London, 1993,* AIP Conf. Proc. **299**, 59 (1994).

38. L. I. Rudakov, A. L. Velikovich, J. Davis, J. W. Thornhill, J. L. Giuliani, Jr., and C. Deeney, Phys. Rev. Lett. **84**, 3326 (2000).

39. A. L. Velikovich, J. Davis, J. W. Thornhill, J. L. Giuliani Jr., L. I. Rudakov, and C. Deeney, Phys. Plasmas **7**, 3265 (2000).

Translated by L. Mosina